

Comparison of tribology performance, particle emissions and brake squeal noise between Cu-containing and Cu-free brake materials

L. Wei^{*}, Y.S. Choy, C.S. Cheung, Henry K. Chu

Department of Mechanical Engineering, The Hong Kong Polytechnic University, Hung Hom, Kowloon, Hong Kong

ARTICLE INFO

Keywords:

Brake squeal noise
Brake wear particle emissions
Disc brakes
Cu-free brake materials

ABSTRACT

The present study developed two Cu-free brake materials using carbon fiber or carbon nanotube as the replacements for copper fiber and evaluated their tribology performance, particle emissions and brake squeal noise. Results show that the coefficients of friction (COFs) of the Cu-free brake materials are lower than that of Cu-containing brake material at the braking conditions with low and medium loads. At the high load braking condition, all the braking materials exhibit comparable COFs. Cu-free brake materials present larger specific wear rates than the Cu-containing brake material. However, the application of carbon fiber can reduce the particle number emission. All brake materials exhibit comparable brake squeal noise.

1. Introduction

The brake materials for passenger vehicles commonly contain 10 to 20 ingredients. Based on the function of each ingredient, they can be classified as binders, reinforcing fibers, fillers and friction additives. The brake materials should satisfy desired tribology performance such as stable friction with low sensitivity to the braking conditions, low wear rate, low brake noise and good fade and recovery performance [1,2]. In addition, the environmental protection requirement is also a driving force for the development of new brake materials. For example, the application of asbestos fiber in brake materials was prohibited by the European nations in 1985 and the United States in 1989 because they are carcinogenic [3].

After 2000, the copper pollution from the vehicle brake systems has become an environmental concern and attracted more and more attention. Copper is a very good ingredient due to its high thermal conductivity and high ductility. The application of copper in the brake materials reduces the intensity of high temperature spots, contributes to form compacted friction layers and stabilizes the variation of coefficient of friction (COF) in the braking process [4,5]. The average contents of copper in the brake pads in the U.S. market and European market are 5% and 10% respectively [6–8]. But copper is toxic to the aquatic organisms and human health. Brake wear particles are one of main sources for the copper pollution. To avoid the toxic effects of Cu-containing wear particles, United States requires a reduction of copper in brake pads to <5% (Cu-low brake pad) by 2021 and < 0.5% (Cu-free brake pad) by 2025

[9].

In recent years, some studies have been conducted on developing Cu-free brake materials. Mahale and Bijwe [1] used the plasma treated and untreated stainless steel swarf (SSS) as the replacement for the copper fiber and reported that the Cu-containing brake materials presented a better performance in wear resistance, but lower fade and recovery COFs than the SSS brake material. In addition, the SSS treated with plasma could further improve the wear resistance by 10% due to the stronger adhesion between the plasma treated SSS and phenolic resin. Mahale et al. [10] used Promaxon-D as the replacement for copper powder in a brake material and found that Promaxon-D can reduce the sensitivity of COF towards speed and contact pressure. But the Cu-containing brake material exhibited a larger COF than the Cu-free brake materials. Tavangar et al. [5] developed a Cu-free brake material using the cellulose fiber and thermal graphite and reported that the COF of the Cu-free brake material is a bit higher than that of the Cu-containing brake material. In our previous study, we manufactured two Cu-free brake materials using the steel fiber or ceramic fiber as the replacement for Cu fiber. The Cu-free brake materials exhibited a comparable tribology performance with the Cu-containing brake material, but they presented higher particle emissions [11].

Among various fibers, carbon fiber and carbon nanotube own a series of excellent properties that can be used in the brake materials. Carbon fibers have the properties of high strength, high modulus, self-lubricating and good thermal stability [12]. Carbon nanotubes have the properties of high stiffness, high thermal resistance and high aspect

* Corresponding author.

E-mail address: long.wei@connect.polyu.hk (L. Wei).

ratio with low density [13,14]. Some previous studies have shown that carbon fiber and carbon nanotube can improve the wear resistance and friction stability of brake materials [15,16]. Moreover, carbon nanotube can reduce the vibration of brake materials [16]. As introduced above, copper fibers also exhibit the similar functions in the brake materials. Therefore, carbon fibers and carbon nanotubes have the potential to replace the copper fiber in the brake materials. Regarding the effects of carbon fiber and carbon nanotube on the tribology performance of brake materials, Ahmadijokani et al. [12,15] analyzed the effects of short carbon fiber on the mechanical properties and tribology performance of brake materials. They found that the application of carbon fiber increased the storage modulus and decreased the damping factor of the brake materials [12]. Moreover, they observed the inclusion of carbon fiber decreased the specific wear rate and COF [15]. Lertwassana et al. [17] developed a aramid pulp and carbon fiber reinforced NAO brake material and found the new developed brake material exhibited a high and stable friction coefficient and good wear resistance. The optimal aramid pulp to carbon fiber mass ratio was 75:25. El-kashif et al. [16] found carbon nanotube could improve the mechanical properties of the brake material, including hardness, strength and modulus. Moreover, they also observed that the use of carbon nanotube could reduce the brake noise and brake material vibration as well as increase the wear resistance of the brake material. As introduced above, both of carbon fiber and carbon nanotube can be regarded as the possible replacements for the copper fiber. However, only a few studies investigated the roles of carbon fiber and carbon nanotube in the Cu-free brake materials.

The present study aims to investigate the tribology performance, brake wear particle emissions and brake squeal noise of two Cu-free brake materials using carbon fiber or carbon nanotube as the replacement for copper fiber and compare them with the Cu-containing brake material. In addition to the copper pollution, particles emitted from the automotive brakes can induce some adverse effects on human health due to their size distribution, chemical composition, surface area, etc [18]. Braking squeal noise is a major issue in automotive industry causing the customer uncomfortableness [19]. Thus, it is necessary to investigate the brake wear particles and brake squeal noise emitted from the new developed Cu-free brake materials. Brake squeal noise involves the whole system dynamic and the local dynamic at the contact surface and the second item includes the impacts between contact asperities and the variation of contact plateaus [20,21]. The replacements of copper fiber with carbon fiber and carbon nanotube affect the size, shape and element compositions of the contact plateaus on the brake pad surface leading to different local dynamics at the contact surface [20,22]. Therefore, the present study investigated the brake squeal noise focusing on the correlation between the characteristics of contact plateaus and the brake squeal noise. We expected the new developed Cu-free brake materials could present appropriate tribology performance as well as comparable brake wear particle emissions and brake squeal noise with Cu-containing brake material.

2. Experimental set-up

2.1. Materials

The Cu-free brake materials were prepared based on a Cu-containing NAO brake material, named as RBM, including 10 ingredients. Its composition is listed in **Table 1** and copper fiber content is 10 vol%. Two Cu-free brake materials, carbon fiber brake material (CABM) and carbon nanotube brake material (CNBM), were prepared by replacing the copper fiber with carbon fiber and carbon nanotube respectively and keeping the other 9 ingredients (named as parent composition) unchanged. The properties of the fibers and the brake materials are listed in **Tables 2** and **3** respectively.

The fabrication of brake materials was carried out in 3 steps. Firstly, to obtain a homogeneous mixture of the ingredients, all the ingredients were mixed with a high-speed mixer equipped with high speed choppers

Table 1
The composition of reference brake material (RBM).

Ingredients	Functions	Amounts (vol%)
Copper fiber (10%)	Reinforcing fiber	30
Aramid pulp		
Steel fiber		
Graphite	Friction additive	20
MoS ₂		
ZrSiO ₄		
Cashew dust		
Phenolic resin	Binder	20
BaSO ₄	Filler	30
Ca(OH) ₂		

Table 2
Specification of fibers (Supplier's data).

Physical properties	PAN based Carbon fiber	Carbon nanotube	Copper fiber
Color	Black	Black	Yellow
Diameter (μm)	6–8	2–5 × 10 ⁻³	150–250
Length (mm)	2–5	1–3 × 10 ⁻²	1–3
Density (g/cm ³)	1.76	2.1	8.94
Tensile strength (MPa)	650	Extremely high	333
Purity	>98%	>98%	>98%

Table 3
Formulations and specifications of brake materials.

Ingredients (vol%)	RBM	CABM	CNBM
Copper fiber	10	–	–
Carbon fiber	–	10	–
Carbon nanotube	–	–	10
Parent composition	90	90	90
Density (g/cm ³)	2.08 ± 0.08	1.75 ± 0.03	1.66 ± 0.02
Hardness (HRM 100)	43 ± 2	42 ± 1	42 ± 1

in a rotating speed of 2000 rpm for 20 min. Secondly, the mixture was compression molded at a curing temperature of 150 °C and a compression pressure of 15 MPa for 10 min. Finally, the mixture was post cured in an oven at a 180 °C for 4 h. Then, pin samples were milled from the mixture and machined to a cubic shape with 10 ± 0.2 mm in length and 7 ± 1 mm in thickness. **Fig. 1** shows the Backscatter electron (BSE) pictures of the pin samples. The densities of pin samples were calculated as the ratio of the pin mass and the pin volume as shown in **Table 3**. It can be observed that all the ingredients were mixed very well, and the fibers are uniformly distributed in the brake materials. A commercial brake disc made of pearlitic grey cast iron was used in the present study with 239 mm in diameter and 9 mm in thickness. The surface hardness of brake discs ranges from 90 to 93 HRB 100.

2.2. Test set-up

A pin-on-disc tribometer was used to conduct braking tests as shown in **Fig. 2**. It has been used and validated to analyze the tribology performance of automotive brake contact pairs [23,24]. It includes a horizontal rotating brake disc and a deadweight loaded brake pad sample (pin). The brake disc was mounted horizontally and driven by a motor at constant rotating speed. Tests were conducted under constant sliding velocity and constant contact pressure which are different from the real driving conditions. But the simplified geometry of pin sample in this tribometer makes it adequate to investigate the novel brake materials without considering the design of disc brakes at the early phase of the material design process [25]. The tangential force was measured with an HBM ZLFC3/20 kg load cell with 1 Hz data sampling rate. Then, the COF was calculated from dividing the measured tangential force by the

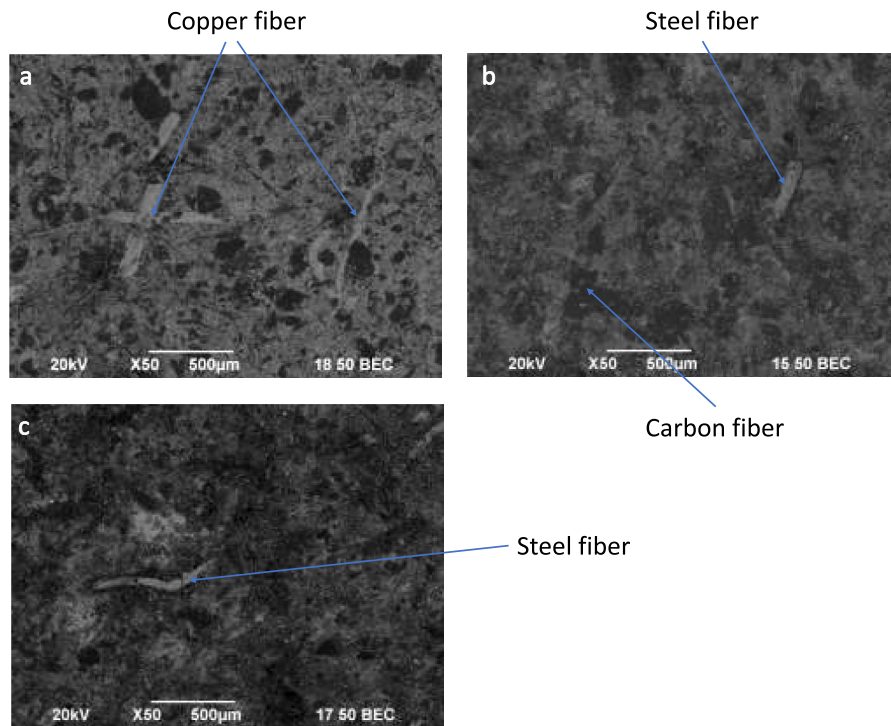


Fig. 1. BSE-SEM pictures of pin samples (a: RBM, b: CABM, c: CNBM).

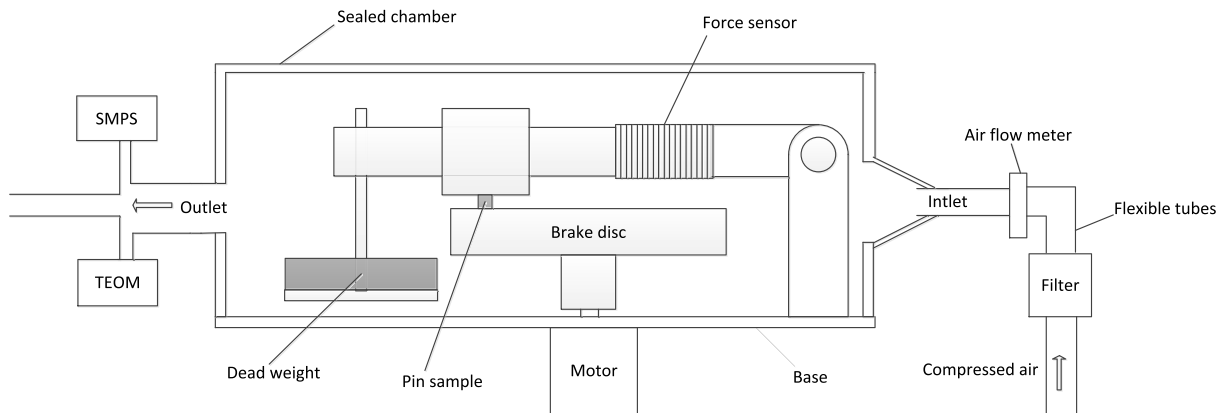


Fig. 2. Schematic of test-rig for tribology performance and airborne particle emissions [11].

applied load. The temperature of pin was measured using a K-type thermocouple placed in a hole inside the pin body with 2 mm away from the pin surface. Pin temperature and tangential force were measured during the whole process of each braking test. The mass of each pin was measured before and after the test using an analytical balance with a sensitivity of 0.01 mg. Then, the wear volumes (m^3) of pin samples were calculated using the densities in Table 3 and the measured mass loss. Finally, the wear of brake material was assessed by the specific wear rate (k_s). It was calculated as [26]:

$$k_s = \frac{\Delta v}{F_N \cdot \Delta s} \quad (1)$$

where k_s (m^2/N) is the specific wear rate; F_N (N) is the applied load; Δs (m) is the sliding distance; ΔV (m^3) is the wear volume of the pin sample. This equation was also used to evaluate the specific wear rate of the brake disc. The wear volumes of brake discs were obtained by measuring

the wear track perpendicularly to the sliding direction with a surface profiler. Three measurements were conducted for each brake disc sample which was cut from the brake disc. A typical cross section surface profile of wear track is shown in Fig. S1 of supplementary information (SI). More information about this tribometer is shown in Ref. [11,27]. Braking tests were carried out at room temperature and humidity. A JEOL Model JSM-6490 scanning electron microscope (SEM) equipped with an energy dispersive X-ray spectroscopy (EDXS) detector was used to investigate the morphology and elemental compositions of friction layers on the pin sample surface as well as the morphology of the brake disc surface. To obtain a repeatable result, eight randomly selected SEM observations were performed for each pin and brake disc.

Fractal dimension is a parameter for the rough surface that reflects its surface roughness. In addition, the value of fractal dimension is independent from the resolution of the measurement instrument and the sample length [28,29]. The brake pad surface roughness affects the

friction and wear behaviours on the contact surface. Therefore, it is necessary to investigate the fractal dimension of the brake pad surface. Fractal dimension (D_s) was calculated as [28]:

$$N(A > a) \sim a^{-(D_s-1)/2} \quad (2)$$

where $N(A > a)$ is the total number of contact plateaus larger than a particular area, a ; D_s is the fractal dimension of a surface. The number and areas of contact plateaus on the pin sample surface were measured using low resolution SEM images ($50 \times$) with a commercial image processing software Image-pro Plus 6.0. In the present study, the smallest area of contact plateau was about $700 \mu\text{m}^2$. Areas smaller than $700 \mu\text{m}^2$ were considered as noise and neglected in counting. The picture processing procedure for measuring the number and areas of contact plateaus is shown in Ref. [27].

Particles emitted from the brake contact pairs were investigated with the tribometer using a closed chamber to control the air cleanliness in it as shown in Fig. 2 [30,31]. The air was introduced into the chamber via an air flow meter and a high efficiency particle absorber (HEPA, Whatman Polycap 36 TF, retention efficiency: 99.97% for particles larger than $0.3 \mu\text{m}$) so that an almost particle-free atmosphere was obtained inside the chamber. Before and after each test, the background particles in the sealed chamber were measured with a scanning mobility particle sizer (SMPS). The background particle concentrations were about $2.6 \#/cm^3$ and hardly impacted the particle measurement. The air in the chamber transported the particles to the outlet (diameter: 50 mm) for the particle measurement. The inlet air velocity was set to 0.28 m/s corresponding to an air flow rate of 47.5 Liter/min which gave an approximate air exchange rate of $94/\text{hr}$. The temperature and humidity of ambient air were about 26°C and $58\text{--}62\%$ respectively which remained constant during the braking tests. The air in the chamber was well mixed because of high air change ratio, the complicated test-rig shape and the rotating of brake disc.

The number and mass concentrations of particles were measured with a scanning mobility particle sizer (SMPS, model 3494) and a

tapered element oscillating microbalance (TEOM, series 1105) respectively, as described in Ref. [11]. SMPS includes a differential mobility analyzer (DMA model 3071A) and a condensation particle counter (CPC model 3022). SMPS measured the particles with the diameters of $15\text{--}750 \text{ nm}$ and provided information of particle number-size distribution, total number concentration (TNC) and geometric mean diameter (GMD). The sampling flow rate for SMPS was 0.3 Liter/min with a sheath air flow of 3 Liter/min . Five measurements were performed for these three parameters in each test. TEOM measured the mass concentration of PM_{10} (PMC) in 1 Hz data recording rate. Its sampling flow rate was in the range of $1\text{--}2.5 \text{ L/min}$. PMC was recorded for 10 min in each test. The detailed information about the equipment for particle measurement is shown in Ref. [11].

Brake squeal noise was investigated with this tribometer as shown in Fig. 3. Pin-on-disc tribometer is adequate to investigate the correlation between the brake squeal noise and local dynamics on the contact surface [11,21]. The sound signal was recorded using a $1/2\text{-inch}$ microphone as shown in Fig. 3. It was placed 10 cm higher than the contact surface and 50 cm away from the center of the brake disc. The analyzed frequency for brake squeal noise was in the range of 1000 to 15000 Hz with a frequency resolution of 25 Hz . The brake squeal noise lower than 1000 Hz was neglected because it was mainly related to the low-frequency structure dynamic. The friction-induced vibration response in tangential and normal directions were measured with two accelerometers installed on the brake pad holder. A 6-channel B&K LAN-XI signal acquisition system was used to record the sound and acceleration signals. The acquired signals were processed with a commercial software PULSE LabShop Version 20.0. The measurement duration for acceleration and sound signals were 30 s and five measurements were conducted in each test. The background noise was measured before and after the test as shown in Fig. S2 of SI. After install the brake pad sample, dead weight and accelerometers, an impact hammer modal test was conducted to identify some natural frequencies of the test rig. The modal test was performed on the brake disc and brake

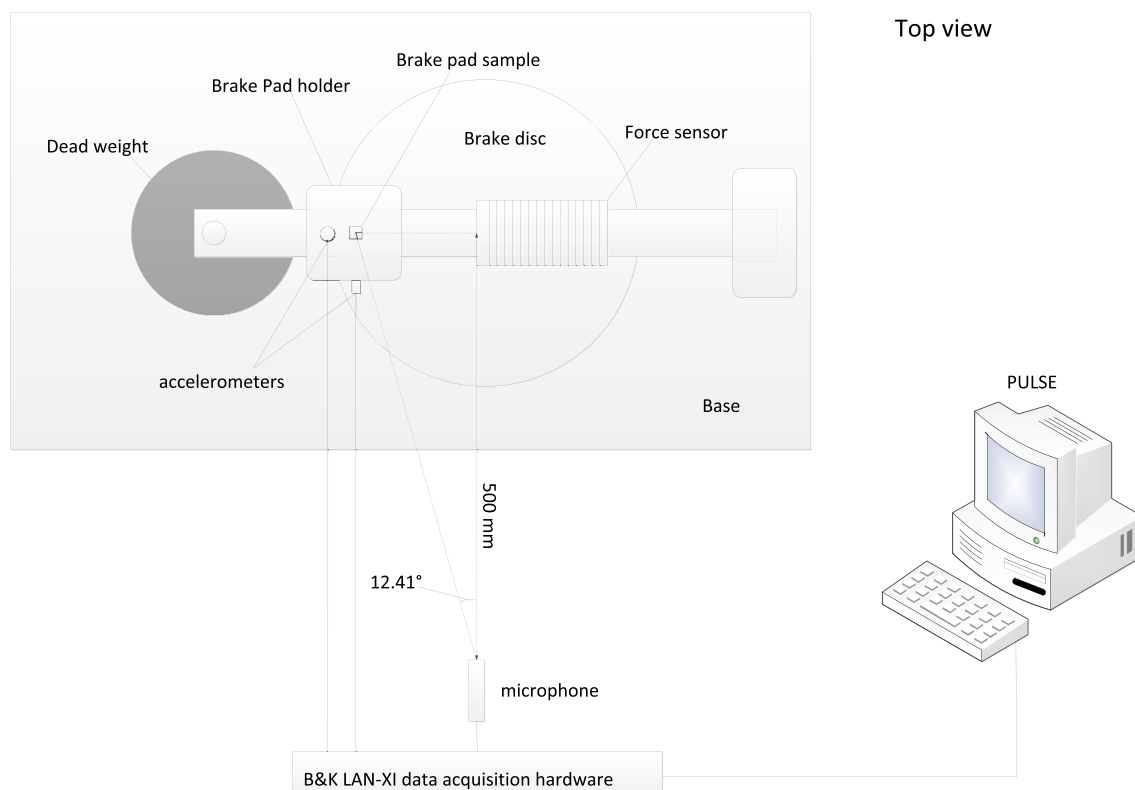


Fig. 3. Schematic of test-rig for brake squeal noise.

pad holder respectively and the relevant frequency response spectra are shown in Figs. S3 and S4 of SI. More information about the brake squeal measurement is shown in Ref. [11].

2.3. Experimental conditions

The applied loads (F_N) were set to 52 (low load), 81 (medium load) and 122 N (high load) correspond to the nominal contact pressures (p) of 0.52, 0.81 and 1.22 MPa. The sliding speed was set to 2.8 m/s. Thus, the experimental $p \cdot v$ values are in the range of 1.46–3.42 MPa m/s, corresponding to the mild wear conditions of the brake pads under urban traffic conditions in which the brake system reduces the vehicle speed but do not stop it [32–34]. Each braking test was performed for 90 min with a new pin sample and the corresponding sliding distance was 15120 m. Braking tests were conducted 3 times to obtain a repeatable result. The mean result is shown in this study. The brake discs after the high load braking test were selected to evaluate their wear conditions. The mean standard errors of the results calculated according to the method in Ref. [35] are shown in Table 4.

3. Results

3.1. Tribology performance

Fig. 4 shows the variation of COF with sliding distance at the low load braking condition. More results at the braking conditions are shown in Fig. S5 of SI. Generally, all the brake materials reach a steady-state stage after a running-in stage. For CNBM at the low load braking condition, it reaches the steady-state stage very fast so that there is no obvious running-in stage. Moreover, CABM and CNBM exhibit comparable durations for the running-in stage at the braking conditions with medium and high loads.

Table 5 shows the mean values and standard deviations of COF at the steady-state stage. RBM exhibits a larger COF than CABM and CNBM at the braking conditions with low and medium loads. At the high load braking condition, all the brake materials exhibit comparable COFs. In addition, the COFs of all the pin samples are in the range for normal braking conditions of motor vehicles [23]. There is a peak value for the COF at the medium load braking condition. When further increasing the applied load, the COF decreases.

The specific wear rates of RBM, CABM and CNBM range from 10^{-15} to $10^{-14} \text{ m}^2/\text{N}$ as listed in Table 5, indicating that all the brake materials exhibit mild wear conditions. CABM and CNBM show larger specific wear rates than RBM. The specific wear rates of brake discs are listed in Table 6 which are in the magnitude of $10^{-16} \text{ m}^2/\text{N}$ indicating the mild wear condition for the brake discs. The brake disc sliding against RBM presents larger specific wear rate than that sliding against CABM and CNBM. It is in agreement with the COF result that RBM presents a larger COF than CABM and CNBM.

Fig. 5 shows the variation of the pin temperature versus sliding distance for all the brake materials. It increases continuously during the whole braking test. Table 5 shows the pin temperatures recorded at the

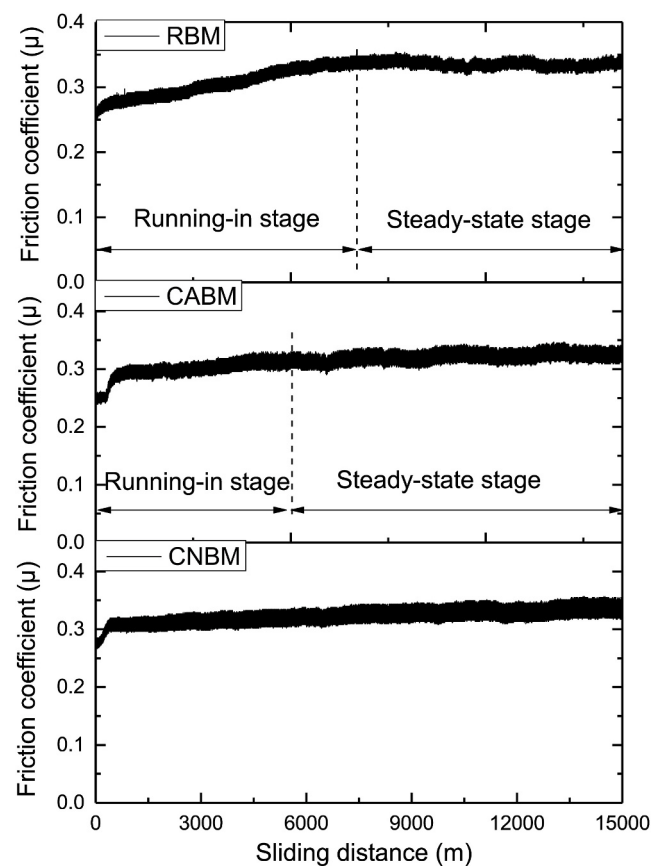


Fig. 4. Variation of friction coefficient during test at the low load braking condition.

Table 5
Friction and wear behaviors of brake materials.

Type of brake material	v m/ s	p MPa	μ (SD)	Δm (SD) $10^{-2}g$	k_s (SD) $10^{-14}\text{m}^2/$ N	T °C	D _s
RBM	2.8	0.52	0.335 (0.008)	0.75 (0.023)	0.45 (0.011)	31.0	2.59
	2.8	0.81	0.434 (0.010)	0.99 (0.026)	0.53 (0.014)	48.7	2.77
	2.8	1.22	0.359 (0.007)	3.44 (0.077)	0.94 (0.021)	54.0	2.65
CABM	2.8	0.52	0.322 (0.012)	1.66 (0.049)	1.21 (0.035)	37.3	–
	2.8	0.81	0.416 (0.015)	1.92 (0.059)	0.91 (0.025)	55.8	–
	2.8	1.22	0.361 (0.022)	2.87 (0.078)	0.90 (0.022)	71.5	–
CNBM	2.8	0.52	0.328 (0.012)	1.15 (0.040)	0.88 (0.021)	32.7	2.49
	2.8	0.81	0.406 (0.020)	3.35 (0.065)	1.68 (0.040)	43.7	2.45
	2.8	1.22	0.354 (0.012)	6.87 (0.031)	2.26 (0.050)	50.8	2.72

SD refers to standard deviation.

end of braking test in the range of 30–75 °C. In the present study, the pin temperatures are lower than 100 °C which are in the range of the brake pad temperature for the mild wear conditions [36].

3.2. Characteristics of worn surfaces

Figs. 6–8 show the morphology of the worn pin surfaces. It can be

Table 4
Average standard errors of results with 95% confidence level.

Parameters	Standard error (%)	Parameters	Standard error (%)
Friction coefficient	3.1	Fractal dimension	1.9
Specific wear rate of brake materials	2.5	Total number concentration	4.6
Specific wear rate of disc	2.8	Particle mass concentration	6.5
Pin sample temperature	3.5	Geometric mean diameter	2.4
A-weighted SPL of brake squeal noise	1.5		

Table 6
Specific wear rates of the brake discs.

Type of brake material	v m/s	P MPa	k_s (SD) $10^{-16} \text{m}^2/\text{N}$
RBM	2.8	1.22	9.54(0.21)
CABM	2.8	1.22	5.03(0.13)
CNBM	2.8	1.22	5.17(0.16)

SD refers to standard deviation.

observed that the morphologies of the worn surfaces are quite different among the brake materials. RBM surface contains a lot of unconnected irregular friction layers. Regarding CABM, the friction layers cover the majority of the worn surface as shown in Figs. 6b and 7b. The fraction of CABM surface covered by friction layers is obviously larger than that of RBM surface. Regarding CNBM, there are some friction layers on the worn surface at the braking conditions with low and medium loads. But the number and areas of the friction layers on the worn surface of CNBM are smaller than those on the worn surfaces of CABM and RBM. After the high load braking test, majority of the pin surface for CNBM is also covered by friction layers. The morphology of the worn surface of CNBM is more complex than that of the CABM and RBM. The matrix surrounding the friction layers on the worn surface of the CNBM suffers severer wear than that on the worn surfaces of the CABM and RBM. Some fibers are extruded from the worn surface as shown in Figs. 6–8. The sizes of the friction layers and the coverage degree of pin surface are increased with increasing the applied load for all the brake materials.

Figs. 9 and 10 show the high-resolution SEM images and EDXS point

spectra of the worn pin surfaces at the braking conditions with low and high loads. More results at the medium load braking condition are shown in Fig. S6 of SI. As shown Fig. 9a, a lot of iron is detected in the friction layers. In addition, the iron concentration in the friction layer is larger than that in the brake material at some sites. At the braking conditions with low and medium loads, copper is detected in a few friction layers which concentration is smaller than that in the brake materials. The low copper content and high iron content in the friction layers indicate many primary plateaus are covered by a film of wear debris at these two braking conditions. Alemani et al. [37] also found a very high iron concentration in the secondary plateaus measured with EDXS which value was even higher than that in the bulk material. At the high load braking condition, the severe adhesion and abrasion wear removes this wear debris film so that more primary plateaus can be detected directly as circled by white line in Fig. 10a. For the CABM, the carbon fiber plays the role in primary plateaus which blocks the movement of wear debris and provides the nucleation sites for the formation of secondary plateaus. For the CNBM, the steel fibers work as the primary plateaus from the EDXS analysis. From the high-resolution SEM images, the compactness of the friction layers of the CNBM is obviously lower than that of the RBM and CABM, as a lot of loosely compacted wear debris can be observed on the worn surface.

The number area distributions of the contact plateaus on the surfaces of RBM and CNBM are shown in Fig. S7 of SI. The fractal dimensions are evaluated from the curve fitting of $N(A>a)$ versus a as shown in Table 5. Fractal dimensions of RBM and CABM are in the range of 2.45–2.77 which are in agreement with our previous studies [11,27]. The average

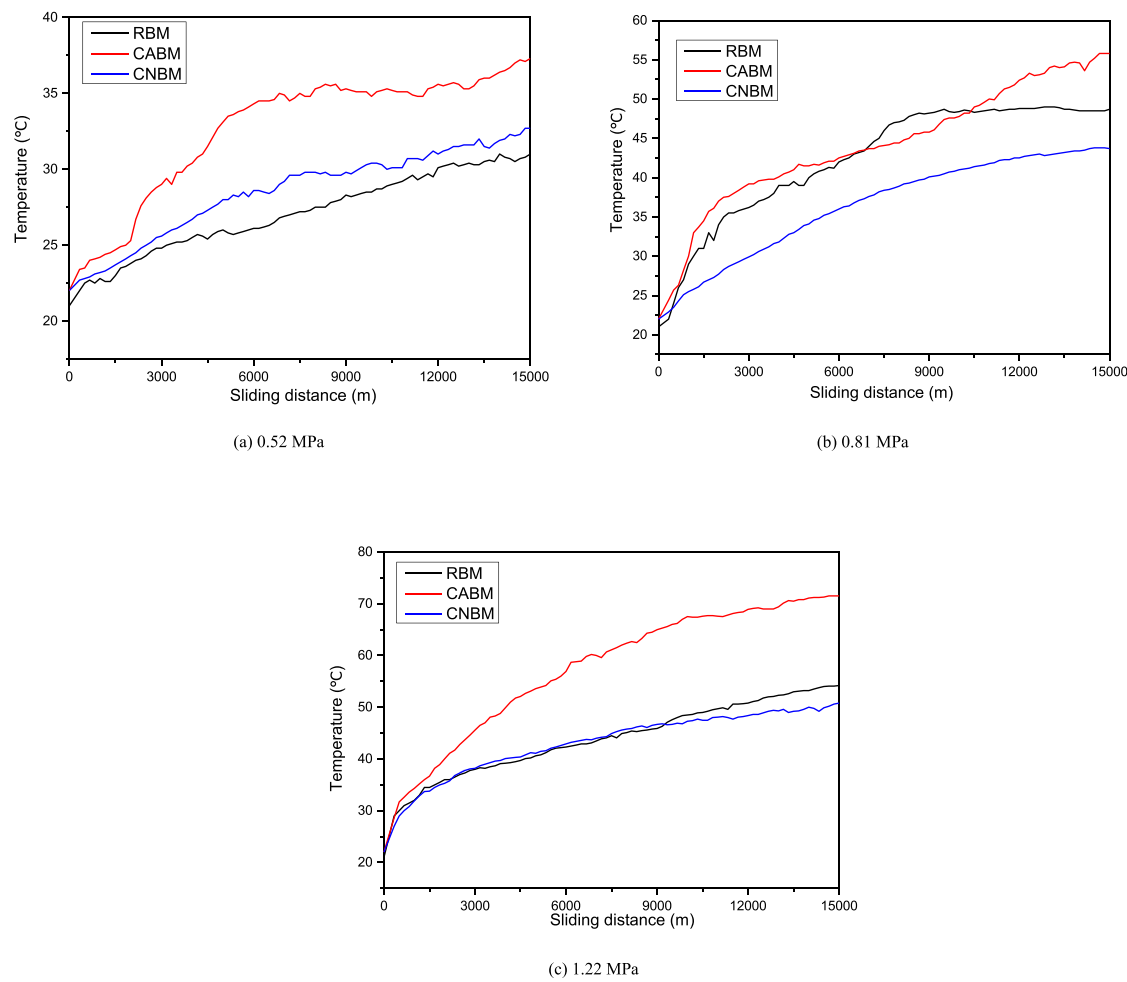


Fig. 5. Variation of pin temperature with sliding distance.

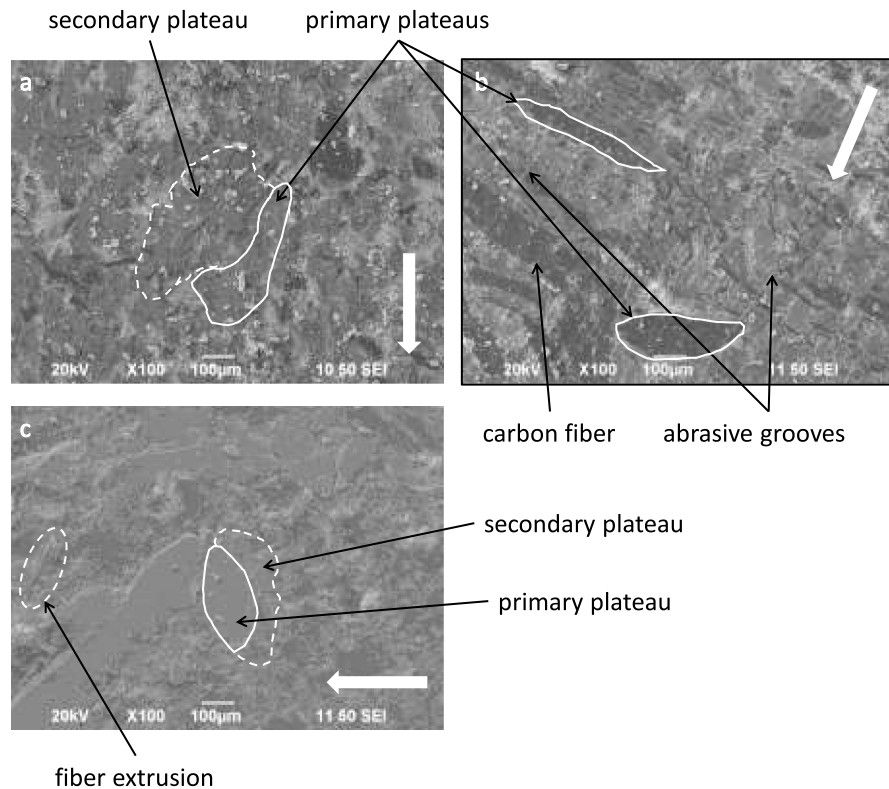


Fig. 6. SEM pictures of the worn pin surfaces at the low load braking condition (a: RBM, b: CABM, c: CNBM; white arrow indicating the sliding direction).

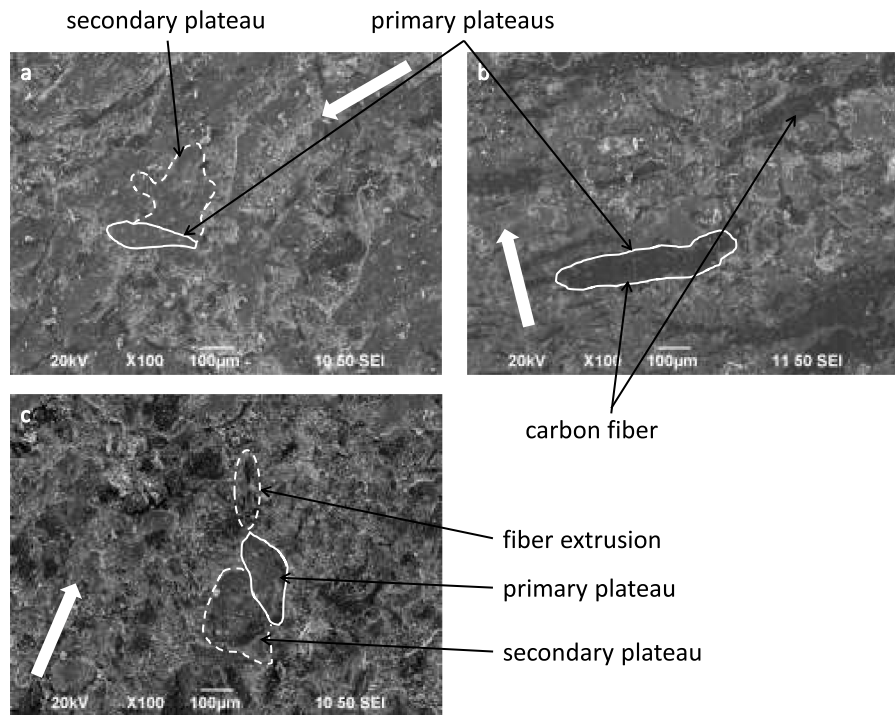


Fig. 7. SEM pictures of the worn pin surfaces at the medium load braking condition (a: RBM, b: CABM, c: CNBM; white arrow indicating the sliding direction).

fractal dimension of CNBM surface is 2.55 which is statistically smaller than that of RBM with the value of 2.67. Fractal dimension is not investigated for the worn surfaces of CABM. This is because the worn surface of the CABM is almost fully covered by the friction layers so that

the number-area distributions of friction layers cannot be measured. Compared with the fractal dimension of the RBM surface, the smaller fractal dimension of the CNBM surface is mainly due to the lack of reinforcing fibers in the CNBM which reduces the areas and number of

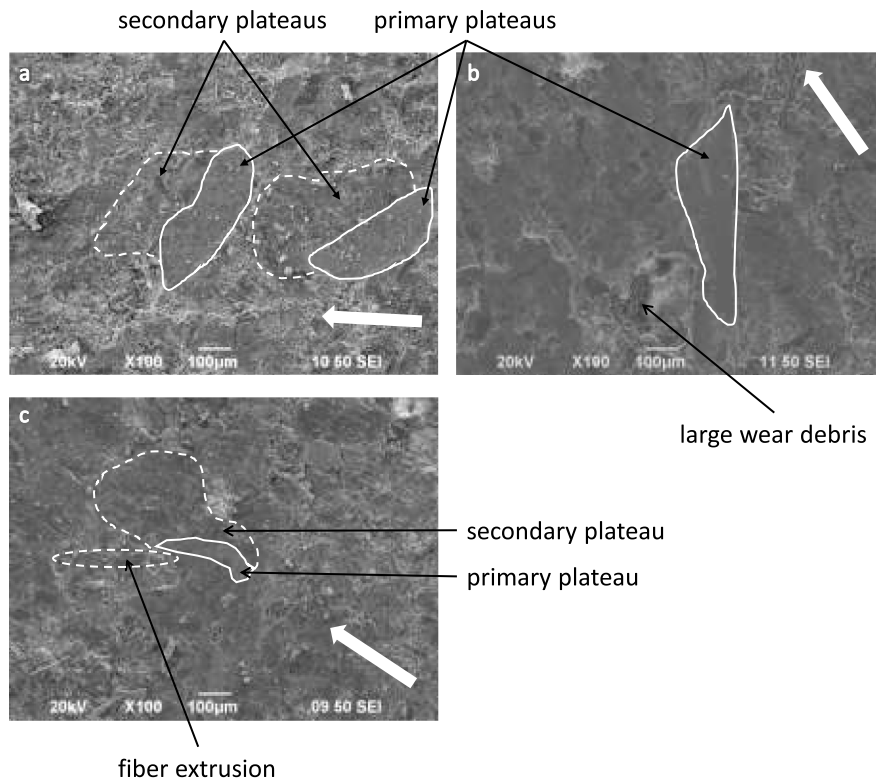


Fig. 8. SEM pictures of the worn pin surfaces at the high load braking condition (a: RBM, b: CABM, c: CNBM; white arrow indicating the sliding direction).

friction layers on the CNBM surface and subsequently decreases the fractal dimension of the CNBM surface. In our previous study [27] the variation of fractal dimension with braking conditions for NAO brake pad surface ranged from 2.46 to 2.59 and its average fractal dimension was 2.51. In another study [11], the average fractal dimensions of steel fiber brake material (STBM) and ceramic fiber brake material (CEBM) surfaces, prepared based on the same RBM, were 2.27 and 2.29 respectively. Thus, the fractal dimensions of CNBM surface are in the reasonable range.

Fig. 11 shows the morphology of the worn surface of brake disc. There are some abrasive grooves on the brake disc surface indicating that the abrasive wear presents a significant role in the brake disc wear. The brake disc sliding against CNBM generates the most abrasive grooves on the brake disc surface. It is because without the coverage of friction layers, a lot of abrasive particles in CNBM are exposed to the brake disc leading to the severest abrasive wear.

3.3. Particle emissions

The number-size distributions of particles at the medium load braking condition are shown in Fig. 12. More results at the other two braking conditions are shown Fig. S8 of SI. The sizes of most particles range from 40 to 300 nm. There are no obvious peaks for all the brake materials at the low load braking condition. But at the braking conditions with medium and high loads, there are several peaks in the range of 70–100 nm.

Table 7 shows the TNC, GMD and PMC results for all the brake materials. The TNC, GMD and PMC increase as increasing the applied load for all the brake materials in most cases. The average TNC results for RBM, CABM and CNBM are 71.2, 56.9 and 94.7 #/cm³ respectively. The GMD ranges from 70 to 130 nm for all the brake materials. The average PMC results for RBM, CABM and CNBM are 163.0, 166.2 and 394.5 μg/m³ respectively.

3.4. Brake squeal characteristics

The brake squeal and vibration spectra at the low load braking condition are shown in Fig. 13. More results at the other two braking conditions are shown in Figs. S9-S10 of SI. The peak's frequency in SPL spectrum matches with the corresponding peak's frequency in vibration spectrum. The peaks in the vibration acceleration spectrum are also coincided with some of the natural frequencies of the test rig as shown in Figs. S3 and S4 of SI. Since the hammer modal test was conducted under the static condition, there are some differences between the peaks in the vibration acceleration spectrum and the peaks in the frequency response spectrum in the modal test. It can be observed that the peaks with the frequencies around 2000 Hz and larger than 10,000 Hz in the tangential acceleration spectrum are larger than those in the normal acceleration spectrum which indicates that the effect of tangential vibration on the brake squeal spectrum is larger than that of normal vibration at this frequency range. It can also be observed that the peaks with the frequencies in the range of 2000–10,000 Hz in the normal acceleration spectrum are larger than those in the tangential acceleration spectrum which indicates that the effect of normal vibration on the brake squeal spectrum is larger than that of tangential vibration at this frequency range. Overall, the contribution of vibration to the brake squeal spectrum is related to the frequency. The relevant A-weighted SPLs of brake squeal noise with standard deviations are shown in Fig. 14. It can be seen that a higher applied load leads to a higher A-weighted SPL of brake squeal noise. It is because the increment of applied load increases the power introduced into the contact leading to more energy dissipated as acoustics [38]. All the brake materials show comparable A-weighted SPLs. But RBM still presents the lowest A-weighted SPL at the braking conditions with medium and high loads.

4. Discussion

The friction and wear behaviors of the brake materials are influenced

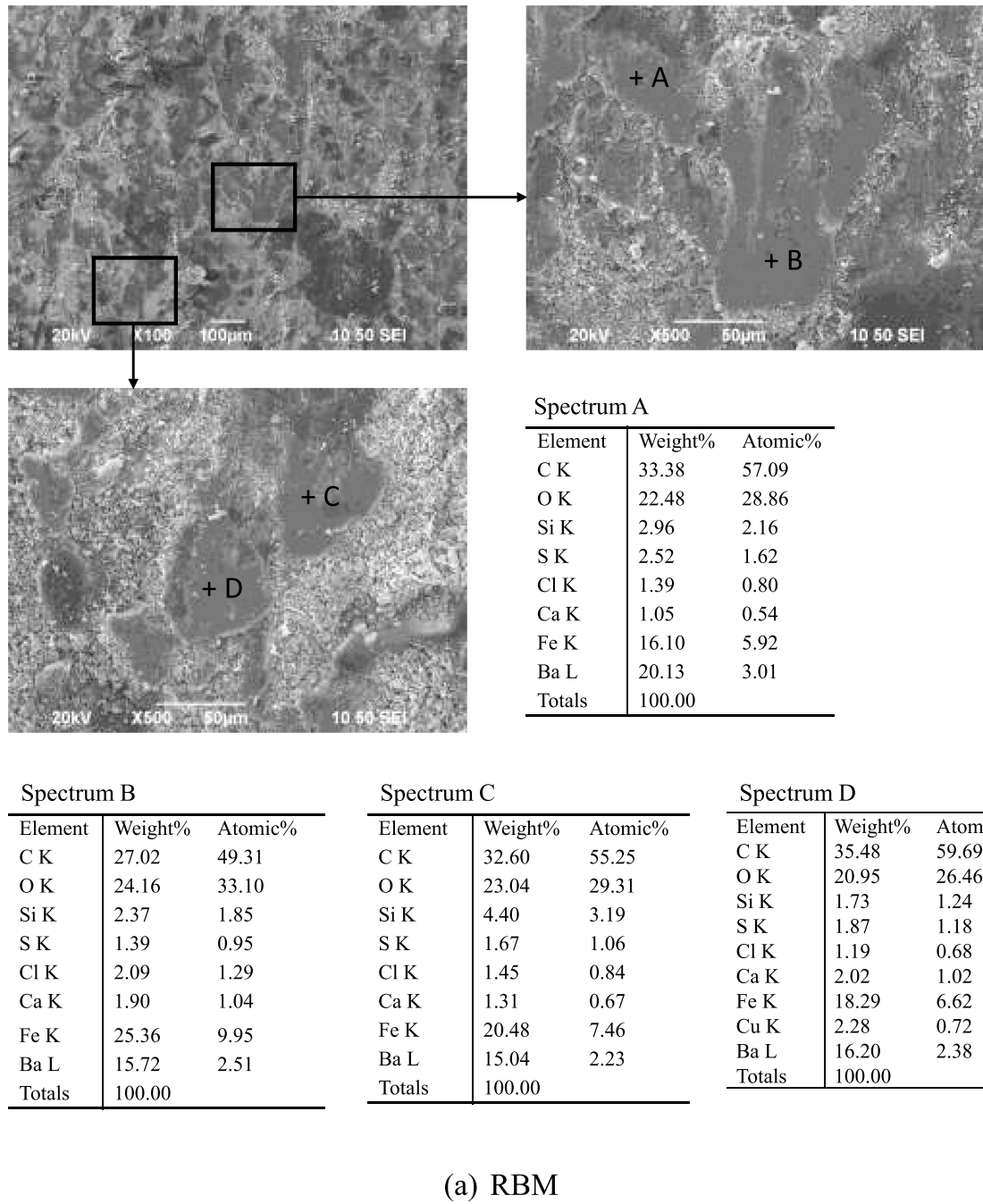


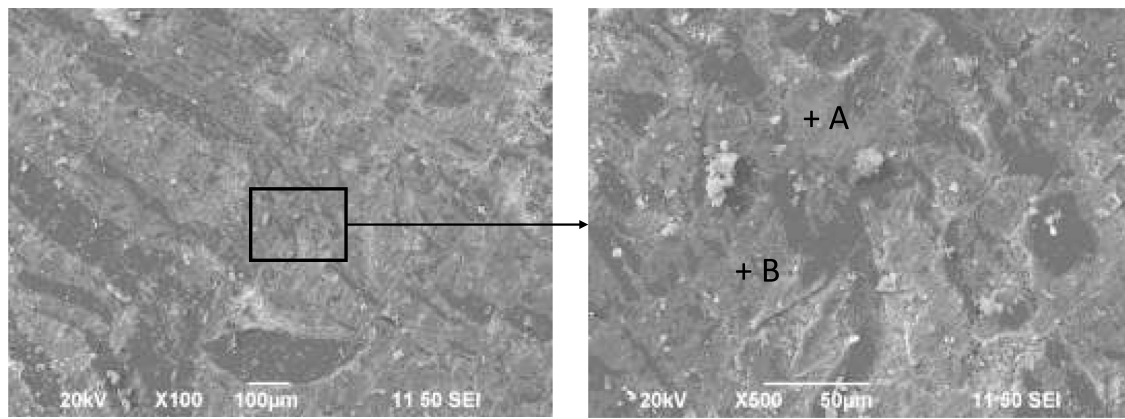
Fig. 9. SEM pictures and EDXS point spectra of the worn pin surfaces at the low load braking condition (a: RBM, b: CABM, c: CNBM).

by the morphologies and element compositions of friction layers, also called contact plateaus, formed on the contact surface [9,39]. Friction layers can be classified into two types. One is the primary plateaus formed by some hard and large ingredients protruding from the pin surface [40]. These protruding primary plateaus form nucleation sites for the growth of the other one, secondary plateaus. The wear debris accumulates and compacts against the primary plateaus to form the secondary plateaus [40].

The running-in stage is the duration for the contact pair to reach a steady friction and wear process on the contact surface. The adhesion and abrasion interactions between the pin and the brake disc surfaces play a dominating role in determining the friction force. Moreover, the

work of adhesion is determined by the ingredients of the mating surfaces. Since both carbon fiber and carbon nanotube are organic fibers and composed of carbon atoms, the adhesive interactions between these two types of fibers and the iron disc are comparable which leads to the comparable durations of the running-in stages for the CABM and the CNBM.

The contact pressure for normal braking conditions is commonly in the scope of 1–3 MPa. If the low-pressure braking condition is included, a peak value of COF can be seen. Friction force is determined by the adhesion and abrasion between contact surfaces. Abrasive interaction is independent from the applied load because it is mainly determined by the attack angle of the abrasive particles [41]. Thus, the variation of



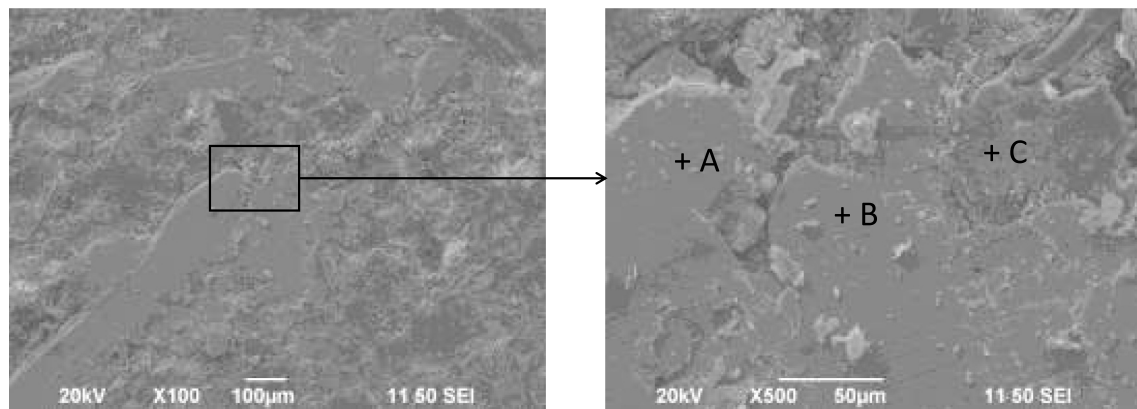
Spectrum A

Element	Weight%	Atomic%
C K	19.15	45.75
O K	18.66	33.47
S K	9.84	8.81
Fe K	3.40	1.75
Ba L	48.95	10.23
Totals	100.00	

Spectrum B

Element	Weight%	Atomic%
C K	68.09	82.77
O K	15.36	14.02
Si K	1.54	0.80
Fe K	5.25	1.37
Ba L	9.76	1.04
Totals	100.00	

(b) CABM



Spectrum A

Element	Weight%	Atomic%
C K	8.42	29.72
Si K	1.06	1.60
Fe K	90.52	68.69
Totals	100.00	

Spectrum B

Element	Weight%	Atomic%
C K	6.40	24.13
Fe K	93.60	75.87
Totals	100.00	

Spectrum C

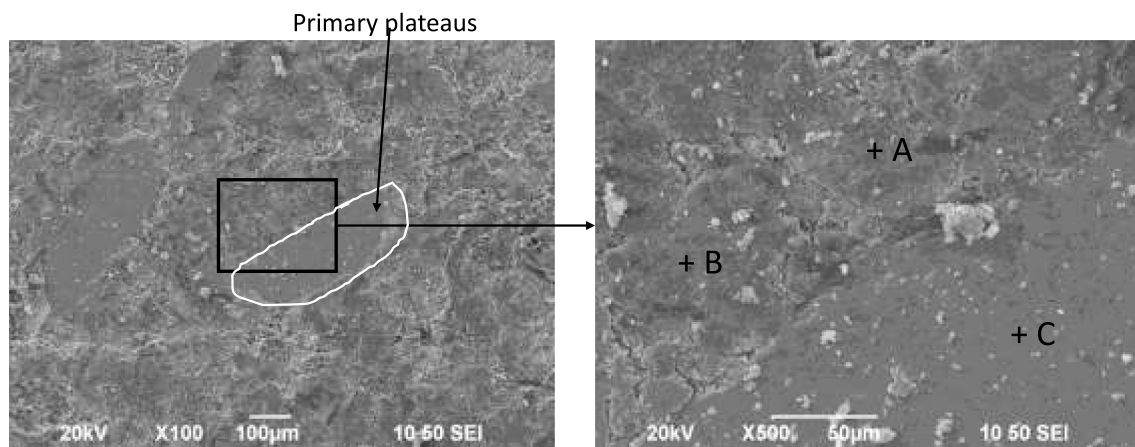
Element	Weight%	Atomic%
C K	24.24	51.97
O K	18.45	29.70
Si K	2.73	2.50
S K	7.94	6.38
Fe K	2.57	1.18
Ba L	44.08	8.27
Totals	100.00	

(c) CNBM

Fig. 9. (continued).

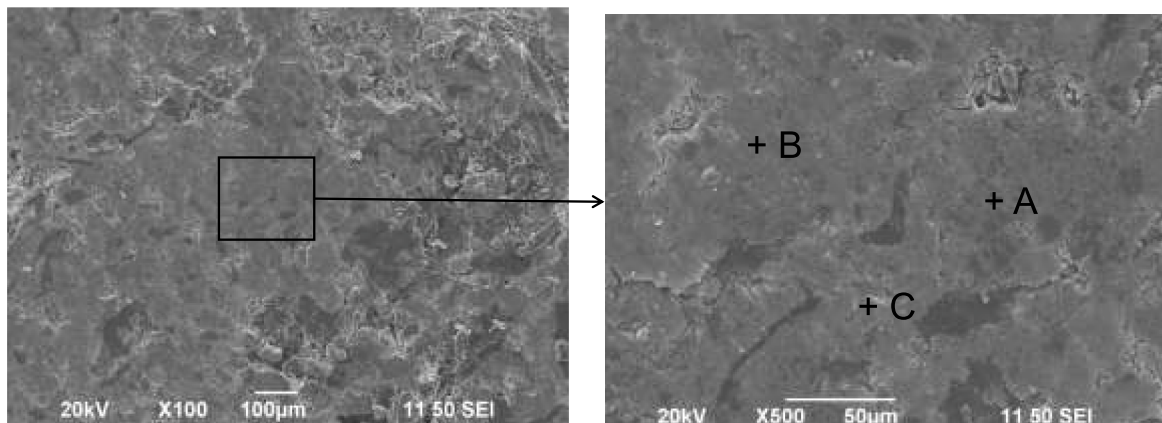
friction force with the applied load is mainly influenced by the adhesive interaction between contact asperities. Regarding the contribution of adhesive interaction to the COF, COF can be expressed as $\text{COF} = \tau_m \cdot A_r / F_N$. Where τ_m is the shear strength of the adhesive bonds between contact asperities that is independent from the applied load; A_r is the real contact area; F_N is the applied load. Under the low-pressure braking

condition, an increase of applied load leads to the formation of new contact plateaus so that the increase of real contact area is larger than the relevant increase of applied load. Therefore, a larger COF is observed. As increasing the applied load from medium to high, the variation of real contact area mainly occurs on the existing contact plateaus [40]. In this contact condition, the increase of real contact area is smaller than the



Spectrum A			Spectrum B			Spectrum C		
Element	Weight%	Atomic%	Element	Weight%	Atomic%	Element	Weight%	Atomic%
C K	25.39	48.11	C K	16.48	38.21	O K	12.49	35.31
O K	24.11	34.31	O K	21.10	36.72	Si K	3.98	6.41
Si K	5.71	4.63	Si K	6.22	6.17	Fe K	7.69	6.23
S K	4.50	3.19	S K	4.40	3.83	Cu K	70.85	50.41
Ca K	2.86	1.62	Ca K	1.65	1.15	Ba L	4.99	1.64
Fe K	5.29	2.16	Fe K	9.72	4.85	Totals	100.00	
Cu K	3.35	1.20	Cu K	3.79	1.66			
Ba L	28.79	4.77	Ba L	36.63	7.43			
Totals	100.00		Totals	100.00				

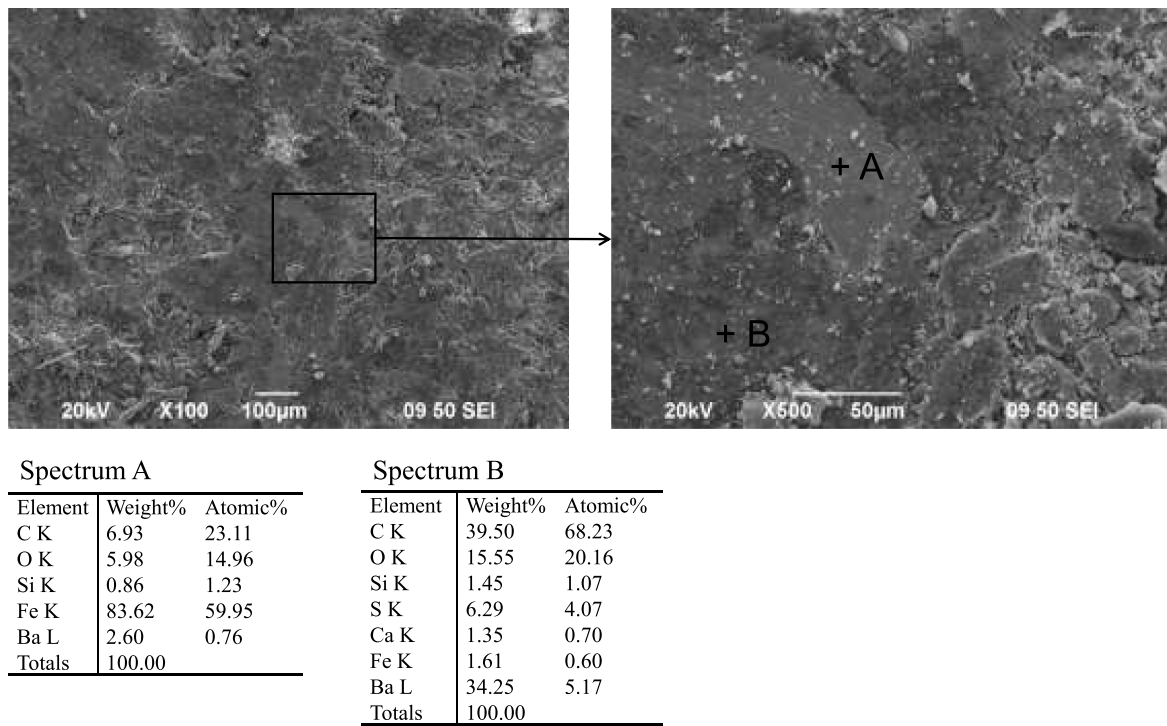
(a) RBM



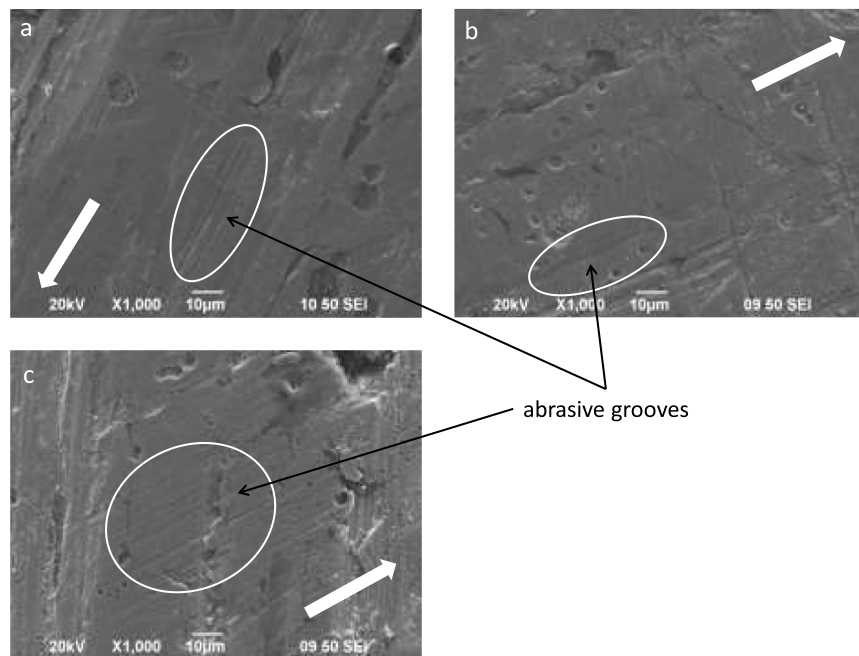
Spectrum A			Spectrum B			Spectrum C		
Element	Weight%	Atomic%	Element	Weight%	Atomic%	Element	Weight%	Atomic%
C K	36.88	62.46	C K	20.88	45.82	C K	8.46	22.61
O K	20.70	26.32	O K	21.01	34.61	O K	19.29	38.69
Si K	2.72	1.97	Si K	1.65	1.55	Si K	6.28	7.17
S K	3.56	2.26	S K	9.34	7.68	S K	3.87	3.87
Ca K	1.35	0.69	Ca K	0.65	0.43	Ca K	2.00	1.60
Fe K	5.32	1.94	Fe K	3.57	1.68	Fe K	35.22	20.24
Ba L	29.46	4.36	Ba L	42.90	8.23	Ba L	24.88	5.81
Totals	100.00		Totals	100.00		Totals	100.00	

(b) CABM

Fig. 10. SEM pictures and EDXS point spectra of the worn pin surfaces at the high load braking condition (a: RBM, b: CABM, c: CNBM).



(c) CNBM

Fig. 10. (continued).**Fig. 11.** SEM pictures of the worn surfaces for brake discs (a: RBM, b: CABM, c: CNBM; white arrow indicating the sliding direction).

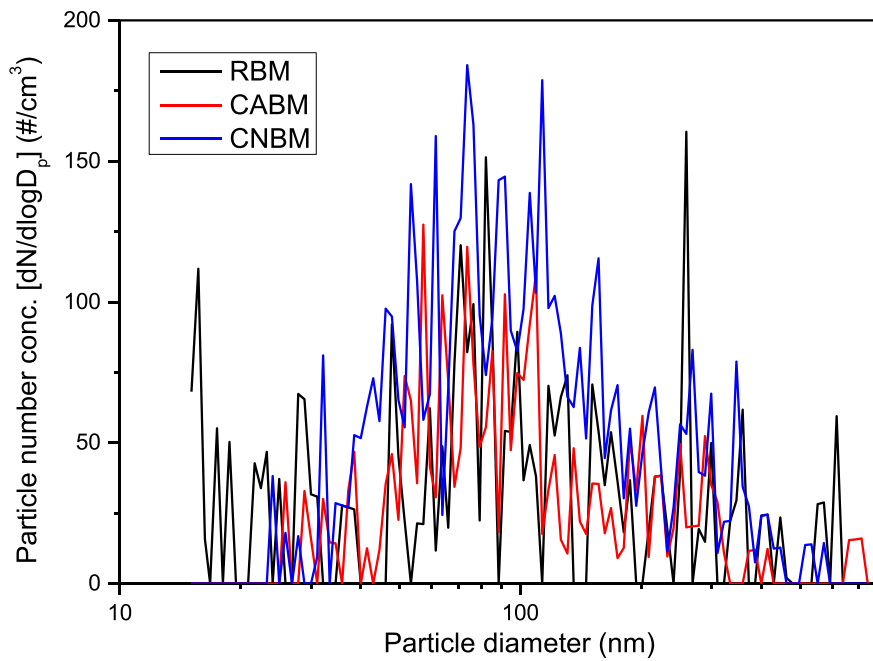


Fig. 12. Particle number size distributions at the medium load braking condition.

Table 7
TNC, GMD and PMC.

Type of brake material	p MPa	TNC (SD) #/cm ³	GMD (SD) nm	PMC (SD) μg/m ³
RBM	0.52	36.4(0.51)	71.8(2.47)	59.8(30.57)
	0.81	55.9(1.43)	87.3(2.58)	119.7(75.73)
	1.22	121.4(1.40)	117.0(2.18)	309.5(52.41)
CABM	0.52	20.5(0.81)	102.97(1.80)	112.78(72.52)
	0.81	44.3(0.55)	97.60(1.81)	170.27(91.33)
	1.22	71.2(3.19)	121.50(1.78)	215.61(101.08)
CNBM	0.52	55.1(1.19)	94.97(2.17)	175.08(102.94)
	0.81	82.7(2.07)	100.65(1.95)	397.97(124.08)
	1.22	146.3(3.11)	106.13(1.97)	610.32(114.80)

SD refers to standard deviation.

related increase of applied load due to the elastic deformation of the real contact area on the contact plateaus which results in a decrease of COF. Regarding the plastic deformation of the real contact area on the contact plateaus, the variation of real contact area is proportional to the applied load which cannot affect the COF [42]. Straffelini et al. [32] also found that a peak in COF was recognized at low loads. Bode et al. [43] found that the COFs of various brake materials under the braking conditions of low contact pressures were lower than those under the braking conditions of normal contact pressures.

Compared with the COF of RBM, the smaller COFs of CABM and CNBM are mainly due to the following two factors. Firstly, carbon fiber and carbon nanotube have lubricating nature that can reduce the COF. Carbon fibers consist of parallel sheets of carbon atoms arranged along the fiber axis which is similar to the structure of graphite so that the adjacent carbon atom sheets can slide relatively to each other [15,44]. This microstructure of carbon fiber leads to lubricating effect. Carbon nanotubes are too small to disperse in the brake materials uniformly as a single fiber. Thus, they are agglomerated as carbon nanotube bundles in the brake material. These carbon nanotube bundles also have lubricating nature [13]. Secondly, the work of adhesion between steel and copper (about 0.83 J/m²) is obviously higher than that between steel and carbon fiber or between steel and carbon nanotube (less than 0.2 J/m²) [42, 45]. Therefore, CABM and CNBM induce less adhesion interaction

between the disc and the pin sample which contributes to the lower COF compared with that of RBM.

The low specific wear rate of RBM is mainly because the plastic deformation of copper fiber can generate soft particles which can enter into the friction layers easily and then improve their mechanical strength [4,46]. As shown in Fig. 6, many abrasive grooves are observed on the friction layers of the CABM at the low load braking condition which indicates that abrasive wear is a significant wear mechanism for CABM. This phenomenon leads to the high specific wear rate of the CABM. For the CNBM, the carbon nanotube is too small to individually work as primary plateaus. Therefore, the secondary plateaus on the CNBM surface are lack of the support of primary plateaus leading to a low shear strength and could be worn out easily. Thus, the CNBM presents the highest specific wear rate among the three brake materials. But the COF can still be kept in the range for normal braking condition where the COF is in the range of 0.3–0.6 [43]. It is because firstly the parent composition already contains 20 vol% of reinforcing fibers that can work as primary plateaus; and secondly, in regions without the coverage of friction layers, the abrasion of the pin surface is enhanced which can increase the friction coefficient.

The CABM presents the highest pin temperature at each braking condition. The CNBM presents the lowest pin temperature at the braking conditions with medium and high loads. The pin temperature is related to the thermal conductivity of the pin sample. Regarding the CNBM, due to the very small size of carbon nanotube, its contribution to the thermal conductivity of the pin sample is quite limited leading to the lowest pin temperature. Regarding the CABM, despite the thermal conductivity of PAN based carbon fiber (ranging from 8 to 70 W/m.K along the axis [47]) is lower than that of copper fiber (384 W/m.K [48]), carbon fiber has higher effect on improving the thermal conductivity of a pin sample than copper fiber. It is because the contact plateaus on the CABM surface is much larger than that on the RBM surface as shown in Figs. 6–8. Large contact plateaus enhance the heat transmission from the contact surface into the pin sample body.

The formation and deterioration of friction layers are closely related to the reinforcing fibers in the brake materials. For RBM, the copper fiber forms the primary plateaus. However, the film of wear debris cover the primary plateaus so that only a few of primary plateaus can be

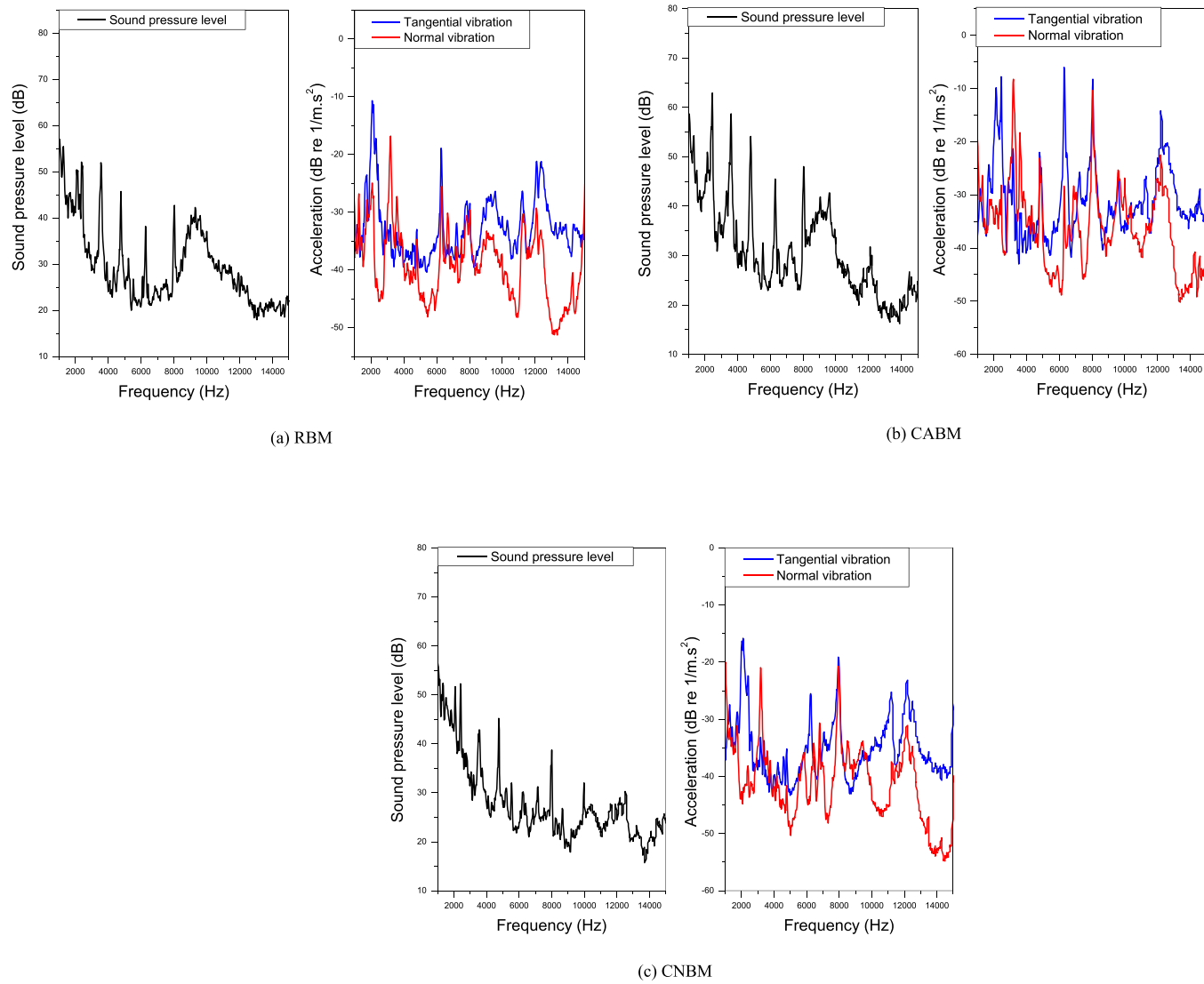


Fig. 13. SPL and acceleration spectra at the low load braking condition.

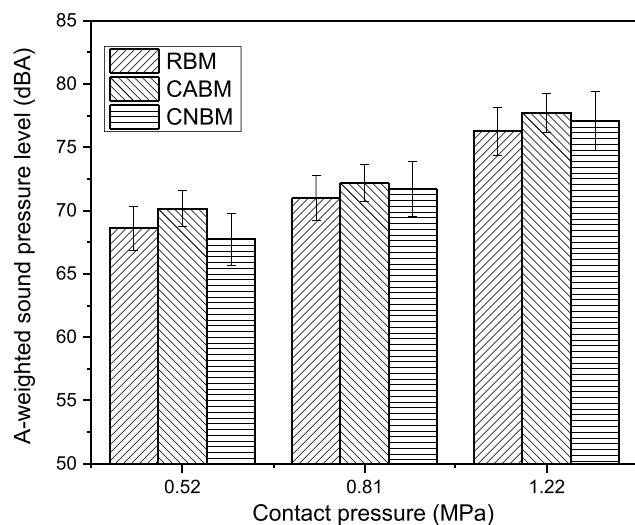


Fig. 14. A-weighted sound pressure level.

detected. Osterle et al. [49] found that the film of wear debris on the brake pad surface had an approximate thickness of 10 μm . For CABM, due to the high strength and flexibility of carbon fibers, they are broken into short fibers or wear debris more difficultly than copper fiber. Some carbon fibers are orthogonal to the sliding direction as shown in Figs. 6–7. Therefore, these carbon fibers work as the primary plateaus as circled in Figs. 6b and 7b that can block the movement of the wear debris leading to the formation of large secondary plateaus. These large secondary plateaus almost fully cover the worn surface. For CNBM, the fewer friction layers on the worn surface of the CNBM than RBM and CABM are mainly due to the lack of reinforcing fibers in the brake material.

A lot of particles consist of iron and iron oxides [50–52]. The iron particles are generated from the abrasion and adhesion wear of the brake disc. The iron oxides are generated from the tribo-oxidation of the brake disc [53,54]. Thus, a large fraction of the particles is in the size range of 40–300 nm. Some particles are produced from the friction layer destruction which characteristics are influenced by the compactness of friction layers. For CABM and CNBM, more particles are produced from the friction layer destruction compared with the RBM due to the lower wear resistance of the contact plateaus on the CABM and CNBM surfaces. Therefore, there are more peaks in the particle number-size distributions for CABM and CNBM. In addition, As increasing the applied load, the

agglomeration process of particles on the contact surface as well as the abrasion wear of pin sample and brake disc are promoted. The promoted agglomeration process for particles can result in a larger particle size [11]. The promoted wear for pin sample and brake disc can result in the larger TNC and PMC results.

The CABM presents the lowest TNC result because some wear debris generated from the disruption of friction layers is too heavy to become particles that can be measured with the SMPS. As shown in Figs. 6–8, the secondary plateaus almost fully cover the worn surface. The wear debris generated from the breakdown of these secondary plateaus has a flaky shape with a large diameter [51]. Therefore, the TNC result of the CABM is lower than that of the RBM despite the specific wear rate of the CABM is higher. For the CNBM, since the friction layers are smaller than those on the CABM surfaces, the wear debris is more easily emitted as particles which contributes to a higher TNC result. Moreover, as shown in Figs. 6–8, the worn surface of the CNBM suffers severer abrasive wear compared with those of the CABM and RBM which also leads to the higher TNC. The large fraction of particle originates from the disruption of friction layers for CABM and CNBM also leads to the large particle size. As listed in Table 7, the GMD results of CABM and CNBM are larger than that of RBM. The average GMDs of RBM, CABM and CNBM are 92.0, 107.4 and 100.6 nm respectively. Since the friction layers on the worn surface of the CABM are larger than those on the worn surface of the CNBM, the particles of CABM present larger diameters than those of CNBM. Lyu et al. [55] investigated the airborne wear particles emitted from two Cu-free brake materials with a pin-on-disc tribometer and an optical particle sizer (OPS) and found that the particle number concentrations of Cu-free brake materials (about 200–250 #/cm³) are much larger than that of Cu-containing brake material (about 90 #/cm³). Gomes Nogueira et al. [56] measured the airborne wear particles emitted from three Cu-free brake materials with a pin-on-disc tribometer and an OPS and reported that the average total number concentration ranged from 200 to 300 #/cm³. Alemani et al. [57] analyzed the influence of braking conditions on the airborne wear particle emissions with a pin-on-disc tribometer and found the friction power was the most important parameter for the airborne wear particle emissions and the mean total number concentration measured with an electrical low pressure impactor (ELPI) varied between 10² and 10⁷ #/cm³. Wahlström et al. [50] investigated the airborne wear particles emitted from a low metallic brake pad under different applied loads with a pin-on-disc tribometer and found the mean concentration of airborne particles measured with a GRIMM was in the range of 150–500 #/cm³.

As shown in Fig. 13 and Figs. S9–S10 of SI, there are large differences in the brake squeal spectra among various brake materials at the same braking condition. The brake squeal spectrum is affected by the friction and wear process [58]. As shown in Figs. 4 and 5, the variation curves of COF and pin temperature are different among different brake materials. Moreover, different reinforcing fibers in the brake materials lead to different number size distributions of friction layers. The number size distribution on the pin surface has significant effect on the amplitude and frequency of the vibration on the contact surface, hence affecting the vibration and brake squeal spectra.

The vibration of test rig can be triggered by the vibration on the contact surface which determines the excited frequencies [59,60]. When pin sample sliding across the brake disc surface, the formation, deformation and deterioration of friction layers as well as the abrasion of the contact surfaces lead to the vibration on the contact surface with wide frequency bands. Rhee et al. [60] called the vibration on the contact surface as the hammering action between the brake pad and the brake disc [61]. A chain reaction of hammering among the components in the brake system can be started by it. When some components are excited into natural modes of vibration, resonance vibration of the brake system will occur, hence generating brake squeal noise.

The low brake squeal noise of RBM is mainly because the soft copper particles, produced from the fracture of copper fiber, can work as solid lubricant and then decrease the vibration amplitude on the contact

surface. Regarding CABM and CNBM, the lubrication nature of carbon fiber and carbon nanotube bundles can also decrease the vibration amplitude on the contact surface contributing to a lower brake squeal noise. However, the friction layers on the CABM surface are larger than those on the CNBM surface. The large friction layer can bear large shear force leading to a larger vibration amplitude on the contact surface and a higher brake squeal noise [20]. Therefore, CABM present a higher brake squeal noise than CNBM at each braking condition.

Cu-free brake materials present lower COFs than Cu-containing brake material at low and medium loads due to the self-lubricating nature of carbon fiber and carbon nanotube. But the specific wear rates of Cu-free brake materials are larger than that of Cu-containing brake material due to the lower wear resistant of friction layers. In addition, Cu-free brake materials show comparable brake squeal noise with Cu-containing brake material. The encouraging outcome is that CABM shows the lowest particle number emission among all the brake materials. Thus, carbon fiber is better than carbon nanotube to replace the copper fiber in the NAO brake materials. Since the specific wear rates of Cu-free brake materials are larger than that of Cu-containing brake material, a further investigation should be performed to improve the formulations of Cu-free brake materials to increase the wear resistant of friction layers and then decrease the specific wear rate.

5. Conclusions

Based on a Cu-containing reference brake material (RBM), two Cu-free brake materials, namely a CABM and a CNBM, were prepared using carbon fiber or carbon nanotube as the replacement for copper fiber. Both Cu-free and Cu-containing brake materials were tested by sliding against an iron disc with a pin-on-disc tribometer. The results can be concluded as follows:

1. The RBM has higher COFs than CABM and CNBM at the braking conditions with low and medium loads. At the high load braking condition, all the brake materials show comparable COFs. RBM exhibits a smaller specific wear rate than CABM and CNBM, but it induces severer wear to the brake disc than CABM and CNBM.
2. The morphologies of worn surfaces of RBM, CABM and CNBM are quite different. The friction layers cover the majority of the CABM surface. Regarding the CNBM, the number and areas of friction layers on the CNBM surface are much smaller than those on the RBM and CABM surfaces. The fractal dimension of CNBM surface is smaller than that of RBM surface.
3. CABM exhibits the lowest TNC result and CNBM presents the highest TNC result. Regarding the particle size, the GMDs of CABM and CNBM are larger than that of RBM.
4. The different brake squeal spectra among the brake materials are mainly due to the different wear processes and the different number size distributions of friction layers on the pin surfaces. But all the brake materials present comparable A-weighted SPLs for brake squeal noise.

CRediT authorship contribution statement

L. Wei: Conceptualization, Methodology, Investigation, Writing - original draft. **Y.S. Choy:** Writing - review & editing, Supervision, Resources, Project administration, Funding acquisition. **C.S. Cheung:** Supervision, Resources. **Henry K. Chu:** Supervision, Resources.

Declaration of competing interest

The authors declare that they have no known competing financial interests or personal relationships that could have appeared to influence the work reported in this paper.

Acknowledgement

The first Author thanks The Hong Kong Polytechnic University for the research studentship (Grant No. RUTT). The authors also thank the funding support from the Research Grants Council of the Hong Kong SAR (Grant No. 15209520).

Appendix A. Supplementary data

Supplementary data to this article can be found online at <https://doi.org/10.1016/j.wear.2020.203577>.

References

- [1] V. Mahale, J. Bijwe, Exploration of plasma treated stainless steel swarf to reduce the wear of copper-free brake-pads, *Tribol. Int.* 144 (2020) 106111.
- [2] R. Vijay, D.L. Singaravelu, R. Jayagathan, Development and characterization of stainless steel fiber-based copper-free brake liner formulation-A positive solution for steel fiber replacement, *Friction* 8 (2020) 396–420.
- [3] J.C. Barrett, P.W. Lamb, R.W. Wiseman, Multiple mechanisms for the carcinogenic effects of asbestos and other mineral fibers, *Environ. Health Perspect.* 81 (1989) 81–89.
- [4] W. Österle, C. Prietzel, H. Kloß, A.I. Dmitriev, On the role of copper in brake friction materials, *Tribol. Int.* 43 (2010) 2317–2326.
- [5] R. Tavangar, H.A. Moghadam, A. Khavandi, S. Banaeifar, Comparison of dry sliding behavior and wear mechanism of low metallic and copper-free brake pads, *Tribol. Int.* (2020) 151.
- [6] B.D. Garg, S.H. Cadle, P.A. Mulawa, P.J. Grobicki, C. Laroo, G.A. Parr, Brake wear particulate matter emissions, *Environ. Sci. Technol.* 34 (2000) 4463–4469.
- [7] H.A.C. Denier van der Gon, J.H.J. Hulskotte, A.J.H. Visschedijk, M. Schaap, A revised estimate of copper emissions from road transport in UNECE-Europe and its impact on predicted copper concentrations, *Atmos. Environ.* 41 (2007) 8697–8710.
- [8] R.M. Harrison, A.M. Jones, J. Gietl, J. Yin, D.C. Green, Estimation of the contributions of brake dust, tire wear, and resuspension to nonexhaust traffic particles derived from atmospheric measurements, *Environ. Sci. Technol.* 46 (2012) 6523–6529.
- [9] M. Leonardi, C. Menapace, V. Matejka, S. Gialanella, G. Straffelini, Pin-on-disc investigation on copper-free friction materials dry sliding against cast iron, *Tribol. Int.* 119 (2018) 73–81.
- [10] V. Mahale, J. Bijwe, S. Sinha, Efforts towards green friction materials, *Tribol. Int.* 136 (2019) 196–206.
- [11] L. Wei, Y.S. Choy, C.S. Cheung, D. Jin, Tribology performance, airborne particle emissions and brake squeal noise of copper-free friction materials, *Wear* 448 (2020) 203215.
- [12] F. Ahmadijokani, A. Shojaei, M. Arjmand, Y. Alaei, N. Yan, Effect of short carbon fiber on thermal, mechanical and tribological behavior of phenolic-based brake friction materials, *Compos. B Eng.* 168 (2019) 98–105.
- [13] H.J. Hwang, S.L. Jung, K.H. Cho, Y.J. Kim, H. Jang, Tribological performance of brake friction materials containing carbon nanotubes, *Wear* 268 (2010) 519–525.
- [14] K.-J. Lee, M.-H. Hsu, H.-Z. Cheng, J.S.-C. Jang, S.-W. Lin, C.-C. Lee, et al., Tribological and mechanical behavior of carbon nanotube containing brake lining materials prepared through sol-gel catalyst dispersion and CVD process, *J. Alloys Compd.* 483 (2009) 389–393.
- [15] F. Ahmadijokani, Y. Alaei, A. Shojaei, M. Arjmand, N. Yan, Frictional behavior of resin-based brake composites: effect of carbon fibre reinforcement, *Wear* 420–421 (2019) 108–115.
- [16] E.F. El-kashif, S.A. Esmail, O.A.M. Elkady, B.S. Azzam, A.A. Khattab, Influence of carbon nanotubes on the properties of friction composite materials, *J. Compos. Mater.* (2019), 0021998319891772.
- [17] W. Lertwassana, T. Parnklang, P. Mora, C. Jubsilp, S. Rimdusit, High performance aramid pulp/carbon fiber-reinforced polybenzoxazine composites as friction materials, *Compos. B Eng.* (2019) 177.
- [18] G. Oberdörster, E. Oberdörster, J. Oberdörster, Nanotoxicology: an emerging discipline evolving from studies of ultrafine particles, *Environ. Health Perspect.* 113 (2005) 823–839.
- [19] N.M. Kinkaid, O.M. O'Reilly, P. Papadopoulos, Automotive disc brake squeal, *J. Sound Vib.* 267 (2003) 105–166.
- [20] S. Lee, H. Jang, Effect of plateau distribution on friction instability of brake friction materials, *Wear* 400–401 (2018) 1–9.
- [21] F. Massi, Y. Berthier, L. Baillet, Contact surface topography and system dynamics of brake squeal, *Wear* 265 (2008) 1784–1792.
- [22] J.W. Kim, B.S. Joo, H. Jang, The effect of contact area on velocity weakening of the friction coefficient and friction instability: a case study on brake friction materials, *Tribol. Int.* 135 (2019) 38–45.
- [23] M. Alemani, Particle Emissions from Car Brakes : the Influence of Contact Conditions on the Pad-To-Rotor Interface [Doctoral Thesis, Comprehensive Summary], KTH Royal Institute of Technology, Stockholm, 2017.
- [24] J. Wahlström, A Study of Airborne Wear Particles from Automotive Disc Brakes [Doctoral Thesis, Comprehensive Summary], KTH Royal Institute of Technology, Stockholm, 2011.
- [25] J. Wahlstrom, Y.Z. Lyu, V. Matjeka, A. Soderberg, A pin-on-disc tribometer study of disc brake contact pairs with respect to wear and airborne particle emissions, *Wear* 384 (2017) 124–130.
- [26] C. Menapace, M. Leonardi, V. Matějka, S. Gialanella, G. Straffelini, Dry sliding behavior and friction layer formation in copper-free barite containing friction materials, *Wear* 398–399 (2018) 191–200.
- [27] L. Wei, Y.S. Choy, C.S. Cheung, A study of brake contact pairs under different friction conditions with respect to characteristics of brake pad surfaces, *Tribol. Int.* 138 (2019) 99–110.
- [28] A. Majumdar, B. Bhushan, Role of fractal geometry in roughness characterization and contact mechanics of surfaces, *J. Tribol.* 112 (1990) 205–216.
- [29] T.R. Thomas, B.G. Rosén, N. Amini, Fractal characterisation of the anisotropy of rough surfaces, *Wear* 232 (1999) 41–50.
- [30] O. Nosko, J. Vanhanen, U. Olofsson, Emission of 1.3–10 nm airborne particles from brake materials, *Aerosol. Sci. Technol.* 51 (2016) 91–96.
- [31] J. Wahlström, M. Leonardi, M. Tu, Y. Lyu, G. Perricone, S. Gialanella, et al., A study of the effect of brake pad scorching on tribology and airborne particle emissions, *Atmosphere* 11 (2020) 488.
- [32] G. Straffelini, L. Maines, The relationship between wear of semimetallic friction materials and pearlitic cast iron in dry sliding, *Wear* 307 (2013) 75–80.
- [33] G. Straffelini, P.C. Verma, I. Metinog, R. Ciudin, G. Perricone, S. Gialanella, Wear behavior of a low metallic friction material dry sliding against a cast iron disc: role of the heat-treatment of the disc, *Wear* 348–349 (2016) 10–16.
- [34] Y. Lyu, J. Wahlström, M. Tu, U. Olofsson, A friction, wear and emission tribometer study of non-asbestos organic pins sliding against AlSiC MMC discs, *Tribology in Industry* 40 (2018) 274–282.
- [35] R.J. Moffat, Describing the uncertainties in experimental results, *Exp. Therm. Fluid Sci.* 1 (1988) 3–17.
- [36] G. Straffelini, S. Verlinski, P.C. Verma, G. Valota, S. Gialanella, Wear and contact temperature evolution in pin-on-disc tribotesting of low-metallic friction material sliding against pearlitic cast iron, *Tribol. Lett.* 62 (2016) 36.
- [37] M. Alemani, S. Gialanella, G. Straffelini, R. Ciudin, U. Olofsson, G. Perricone, et al., Dry sliding of a low steel friction material against cast iron at different loads: characterization of the friction layer and wear debris, *Wear* 376–377 (2017) 1450–1459.
- [38] A. Lazzari, D. Tonazzi, F. Massi, Squeal propensity characterization of brake lining materials through friction noise measurements, *Mech. Syst. Signal Process.* 128 (2019) 216–228.
- [39] M. Eriksson, F. Bergman, S. Jacobson, On the nature of tribological contact in automotive brakes, *Wear* 252 (2002) 26–36.
- [40] M. Eriksson, S. Jacobson, Tribological surfaces of organic brake pads, *Tribol. Int.* 33 (2000) 817–827.
- [41] G. Straffelini, M. Pellizzari, A. Molinari, Influence of load and temperature on the dry sliding behaviour of Al-based metal-matrix-composites against friction material, *Wear* 256 (2004) 754–763.
- [42] G. Straffelini, Friction and Wear: Methodologies for Design and Control, Springer, 2015.
- [43] Bode K, Schramm T, Perzborn N, Raczek S, Münchhoff J, Ostermeyer G-P. LOW μ at LOW PRESSURE – POTENTIAL for REDUCING RESIDUAL DRAG? EuroBrake 2014. Lille, France2014.
- [44] B.K. Satapathy, J. Bijwe, Performance of friction materials based on variation in nature of organic fibres: Part I. Fade and recovery behaviour, *Wear* 257 (2004) 573–584.
- [45] E. Rubinowicz, Friction and Wear of Materials, second ed., Wiley, New York, 1995.
- [46] Y.S. Zhang, Z. Han, K. Wang, K. Lu, Friction and wear behaviors of nanocrystalline surface layer of pure copper, *Wear* 260 (2006) 942–948.
- [47] H.O. Pierson, Handbook of Carbon, Graphite, Diamonds and Fullerenes: Processing, Properties and Applications, William Andrew, 2012.
- [48] H.S. Tekce, D. Kumluatas, I.H. Tavman, Effect of particle shape on thermal conductivity of copper reinforced polymer composites, *J. Reinforc. Plast. Compos.* 26 (2016) 113–121.
- [49] W. Österle, I. Dörfel, C. Prietzel, H. Rooth, A.L. Cristol-Bulthé, G. Degallaix, et al., A comprehensive microscopic study of third body formation at the interface between a brake pad and brake disc during the final stage of a pin-on-disc test, *Wear* 267 (2009) 781–788.
- [50] J. Wahlström, L. Olander, U. Olofsson, A pin-on-disc study focusing on how different load levels affect the concentration and size distribution of airborne wear particles from the disc brake materials, *Tribol. Lett.* 46 (2012) 195–204.
- [51] J. Wahlström, L. Olander, U. Olofsson, Size, shape, and elemental composition of airborne wear particles from disc brake materials, *Tribol. Lett.* 38 (2010) 15–24.
- [52] J. Kukutschová, V. Roubíček, M. Mašláň, D. Jančík, V. Slovák, K. Malachová, et al., Wear performance and wear debris of semimetallic automotive brake materials, *Wear* 268 (2010) 86–93.
- [53] W.M. Rainforth, A.J. Leonard, C. Perrin, A. Bedolla-Jacuinde, Y. Wang, H. Jones, et al., High resolution observations of friction-induced oxide and its interaction with the worn surface, *Tribol. Int.* 35 (2002) 731–748.
- [54] H. So, D.S. Yu, C.Y. Chuang, Formation and wear mechanism of tribo-oxides and the regime of oxidative wear of steel, *Wear* 253 (2002) 1004–1015.
- [55] Y. Lyu, M. Leonardi, J. Wahlström, S. Gialanella, U. Olofsson, Friction, wear and airborne particle emission from Cu-free brake materials, *Tribol. Int.* 141 (2020) 105959.
- [56] A.P. Gomes Nogueira, D. Carlevaris, C. Menapace, G. Straffelini, Tribological and emission behavior of novel friction materials, *Atmosphere* 11 (2020) 1050.
- [57] M. Alemani, J. Wahlström, U. Olofsson, On the influence of car brake system parameters on particulate matter emissions, *Wear* 396–397 (2018) 67–74.

- [58] A. Papinniemi, J.C.S. Lai, J. Zhao, L. Loader, Brake squeal: a literature review, *Appl. Acoust.* 63 (2002) 391–400.
- [59] G. Lacerra, M. Di Bartolomeo, S. Milana, L. Baillet, E. Chatelet, F. Massi, Validation of a new frictional law for simulating friction-induced vibrations of rough surfaces, *Tribol. Int.* 121 (2018) 468–480.
- [60] S. Rhee, P. Tsang, Y. Wang, Friction-induced noise and vibration of disc brakes, *Wear* 133 (1989) 39–45.
- [61] G. Chen, Z. Zhou, P. Kapsa, L. Vincent, Effect of surface topography on formation of squeal under reciprocating sliding, *Wear* 253 (2002) 411–423.